INSTITUTE OF PHYSICS PUBLISHING JOURNAL OF PHYSICS: CONDENSED MATTER

J. Phys.: Condens. Matter **16** (2004) 1927–1938 PII: S0953-8984(04)71816-0

Three-dimensional magnetic ordering in the Rb_2CuCl_4 layer perovskite—structural correlations

F Aguado[1], F Rodríguez[1,4], R Valiente[2], A Señas[1] and I Goncharenko[3]

[1] DCITIMAC, Facultad de Ciencias, Universidad de Cantabria, Santander 39005, Spain
[2] Departamento de Física Aplicada, Universidad de Cantabria, Santander 39005, Spain
[3] Laboratoire Léon Brillouin, CEA-CNRS, Saclay, 91191 Gif sur Yvette, France

E-mail: rodriguf@unican.es

Received 12 November 2003
Published 12 March 2004
Online at stacks.iop.org/JPhysCM/16/1927 (DOI:10.1088/0953-8984/16/12/003)

Abstract

This work investigates the magnetic structure of Rb_2CuCl_4 as a function of pressure and temperature using neutron diffraction. As in most A_2CuCl_4 layered perovskites, there is a 2D ferromagnetic order within the layers. This behaviour is due to the Jahn–Teller (JT) antiferrodistortive structure of the $CuCl_6$ units. Rb_2CuCl_4 undergoes a 3D magnetic transition at $T_N = 16$ K, which mainly depends on the weak antiferromagnetic interlayer interaction. The pressure slightly increases T_N, as $\partial T_N/\partial P = 0.13$ K kbar^{-1}. This behaviour is interpreted in terms of pressure-induced tilts and reduction of interlayer distance, both effects increasing the antiferromagnetic exchange coupling between layers. The results are compared with previous magnetic studies under chemical and hydrostatic pressure along layered perovskites series of $[C_nH_{2n+1}NH_3]_2CuCl_4$ ($n = 1$–3) and $BMnF_4$ (B = Li, Na, K, Rb, Tl, Cs and NH_4) involving JT ions of Cu^{2+} and Mn^{3+}, respectively. We show that the ratio of the interlayer to intralayer coupling, and thus the nature of the magnetic order, can be tuned by chemical or hydrostatic pressure along the A_2CuCl_4 series. The present findings stress the relevance of octahedral tilts on the magnetic behaviour of layered perovskites.

1. Introduction

Layered perovskites A_2CuX_4 (A = K, Rb, Cs, $C_nH_{2n+1}NH_3$; X = F, Cl) and the isomorphous compounds $BMnF_4$ (B = Li, Na, K, Rb, Tl, Cs and NH_4) involve an ample variety of interesting physical phenomena related to the Jahn–Teller (JT) Cu^{2+} and Mn^{3+} ions ($3d^9$ and $3d^4$ configurations, respectively) [1–23]. The axially elongated $CuCl_6$ (or MnF_6) octahedra display an intralayer antiferrodistortive (AFD) structure that is characterized by the alternation

[4] Author to whom any correspondence should be addressed.

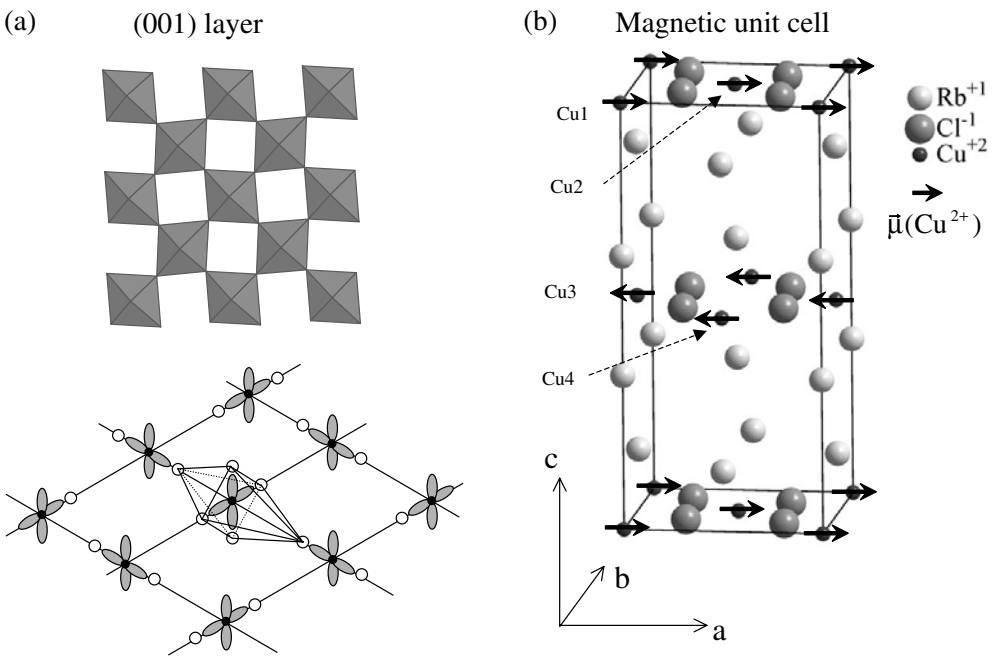

Figure 1. (a) A schematic view of the layered structure of Rb_2CuCl_4 showing the antiferrodistortive structure of the Jahn–Teller distorted $CuCl_6$ octahedra. The drawn orbitals correspond to the unpaired electrons $x^2 - z^2$ and $y^2 - z^2$. The local x, y and z axes are taken along the orthorhombic (*Acam*) crystal directions: **a**, **b** and **c**, respectively. (b) The magnetic structure derived from neutron powder diffraction (see table 3).

of $d_{x^2-z^2}$ and $d_{y^2-z^2}$ orbitals in the plane (figure 1). In copper halide perovskites having Cu–Cl–Cu angles close to 180° (nearly ideal perovskite), the AFD structure is responsible for the intralayer ferromagnetic exchange interaction between nearest Cu^{2+} ions [24]. In contrast, the interlayer exchange interaction is about three or four orders of magnitude weaker, and can be ferromagnetic or antiferromagnetic depending on the relative layer disposition [1]. There has been an intense activity in order to modify material properties on the basis of the search for either new insulating ferromagnets [4, 12, 13, 15–20] or pressure-induced disappearance of the AFD structure [8–11, 14]. Such activity has been focused on both Cu^{2+}- and Mn^{3+}-related compounds, though no indication of bulk ferromagnetism beyond $(CH_3NH_3)_2CuCl_4$ [1] and $CsMnF_4$ [23] has been found. The application of either chemical or hydrostatic pressure tends to destroy the ferromagnetic ordering at the expense of an increase of the antiferromagnetic coupling. Pressure induces a switch from ferromagnetism to antiferromagnetism in $(CH_3NH_3)_2CuCl_4$ [8] and $CsMnF_4$ [25, 26] and an increase of T_N.

Despite the intense research carried out on these compounds, it must be noted that the structural requirements leading to interlayer ferromagnetic coupling in Cu^{2+} compounds are still unknown. Moreover, the two series provide a distinct approach to deal with this problem. In $(C_nH_{2n+1}NH_3)_2CuCl_4$ a change of the 3D magnetism from antiferro- to ferromagnetism is attained on passing from $n = 2$ or 3 to 1 (table 1). In this series, the most remarkable structural change is the reduction of the interlayer distance with the alkylammonium size: 12.33 Å ($n = 3$), 10.59 Å ($n = 2$) and 9.27 Å ($n = 1$). An opposite behaviour is observed in $BMnF_4$ whose in-plane magnetic structure changes from ferromagnetic in

Table 1. Structural and magnetic parameters of the A_2CuCl_4 and A_2CuF_4 series. Parameters d, d_1, d_2 and α represent the interlayer distance, the intralayer Cu–Cu distance, the interlayer Cu–Cu distance, and the tilting angle, respectively. Parameters J and J' correspond to the intralayer and interlayer exchange constant, respectively.

Compound	d (Å)	d_1 (Å)	d_2 (Å)	T_{crit} (K)	α (deg)	J/k (K)	J'/J	Ref.
K_2CuF_4	6.350	2.934	6.70	6.25	170.7	10.0–11.2	$(2.1–7.8) \times 10^{-4}$	[2, 27–29]
Rb_2CuF_4	6.640	4.150	6.97	6.05	—	12.3	—	[2, 3]
Cs_2CuF_4	6.355	4.142	7.00	6.05/9.8	—	8.3–12.6	—	[2, 3, 30]
Rb_2CuCl_4	7.753	5.047	8.535	16	180	18.8	-8×10^{-3}	[31], this work
$(NH_4)_2CuCl_4$	7.730	5.090	8.907	11.2	180	17.0	-3.2×10^{-3}	[31, 32]
$(CH_3NH_3)_2CuCl_4$	9.275	5.247	9.990	8.91	165.10	19.2	5.5×10^{-4}	[1, 33, 34]
$(C_2H_5NH_3)_2CuCl_4$	10.59	5.205	11.219	10.17	169.6	18.6	-8.5×10^{-4}	[1, 33]
$(C_3H_7NH_3)_2CuCl_4$	12.33	5.297	12.886	7.65	166.5	16.0	-6×10^{-5}	[1, 35]
$(C_6H_5NH_3)_2CuCl_4$	15.05	5.205	15.130	—	164.4	25.0	—	[36]
$[C_6H_5(CH_2)_2NH_3]_2CuCl_4$	8.05	5.14	8.11	31.5	166.4	23.0	−0.595	[37, 38]
$[C_6H_5(CH_2)_3NH_3]_2CuCl_4$	9.09	5.28	8.94	14.9	165.7	13.0	-1.03×10^{-2}	[4, 37–39]
$(NH_3CH_2NH_3)CuCl_4$	11.890	5.11	12.43	18.7	170.4	18.7	-5.7×10^{-3}	[36]

Table 2. Structural and magnetic parameters of the $BMnF_4$ series. a, b and c (and β) are the lattice parameters; d_1, d_2 represent the interlayer and intralayer Cu–Cu distances; and α is the Mn–F–Mn tilting angle. J is the intralayer exchange constant, and T_C or T_N refers to the critical temperature. Note that $CsMnF_4$ is the unique ferromagnet of the series.

Compound	Space group	a (Å)	b (Å)	c (Å)	β (deg)	R^1_{eq} (Å)	R^2_{eq} (Å)	R_{ax} (Å)	α (deg)	d_1 (Å)	d_2 (Å)	J/k (K)	T_C/T_N (K)	Ref.
$NaMnF_4$	$P2_1/a$	5.736	4.892	7.748	108.07	1.869	1.808	2.167	138.4	3.774	5.736	—	13	[19]
$CsMnF_4$	$P4/nmm$	7.9440	9.9440	6.3376	—	1.816	1.924	2.095	159.9	3.972	6.338	—	18.9	[40]
$RbMnF_4$	$P2_1/a$	7.8119	7.7761	6.0469	90.443	1.802	1.960	2.108	150.3	3.888	6.047	—	3.7	[40]
						1.824	1.920	2.094	145.5					
$KMnF_4$	$P2_1/a$	7.7062	7.6568	5.7889	90.434	1.808	1.923	2.102	146.4	3.828	5.789	—	5.2	[40]
						1.806	1.910	2.134	140.1					
$LiMnF_4$	$P2_1/a$	5.694	4.629	5.414	113.24	1.817	1.868	2.136	132.6	3.667	5.414	—	—	[41]
$TlMnF_4$	$I2/a$	5.397	5.441	12.484	90.19	1.78	1.86	2.15	146.5	3.832	6.242	−0.45	4.2	[18]

$CsMnF_4$ to antiferromagnetic in $RbMnF_4$, $KMnF_4$, $TlMnF_4$ and $NaMnF_4$ [17] (table 2). Therefore, the intralayer exchange between Mn^{3+} neighbours mainly governs the magnetic behaviour in Mn^{3+}-compounds. According to correlations given by Palacio *et al* [17], the intralayer Mn–F–Mn tilt angle, α, is the main structural parameter driving the sign of the magnetic interactions. Thus ferromagnetic exchange is favoured whenever α is greater than the critical angle, $\alpha_C = 147°$ [26]. $CsMnF_4$ and some Mn^{3+} ions in $RbMnF_4$ accomplish such structural requirements, and so exhibit ferromagnetic behaviour [26]. Contrary to Cu^{2+}-related perovskites, the disappearance of 3D ferromagnetic ordering in Mn^{3+}-perovskites is accompanied by a decrease of the interlayer distance (tables 1 and 2). Pressure experiments showed that the enhancement of the antiferromagnetic interactions at the expense of the ferromagnetic ones is due to an increase of α with pressure [26]. Unfortunately, the lack of structural and magnetic studies in copper perovskites and, in particular, about the local structure around the JT ion, precludes any attempt from establishing magneto-structural correlations in these compounds under pressure. Furthermore, pressure investigations carried out on the isomorphous K_2CuF_4 revealed a pressure-induced transition from ferromagnetism to antiferromagnetism due to a crystal-structure change involving rearrangement of the CuF_6

octahedra from AFD to ferrodistortive [42–45]. It has been shown that the application of pressure to these compounds reduces the axial elongation, yielding a partial reduction of the JT effect in $CuCl_6^{4-}$ [6, 12, 14]. However, experimental studies devoted to understanding the structural variations with pressure and how they affect the magnetic ordering are at present very scarce.

This work investigates the crystal and magnetic structures of Rb_2CuCl_4 as a function of pressure by neutron powder diffraction (NPD). Chlorides have a great advantage with respect to fluorides for structural and magnetic studies under pressure due to their higher compressibility. Among A_2CuCl_4 layered compounds, Rb_2CuCl_4 is interesting since it is the only member of the series providing interlayer distances shorter than those of the $(CH_3NH_3)_2CuCl_4$ ferromagnet. In particular, Rb_2CuCl_4 is antiferromagnetic although it presents the shortest interlayer distance. Moreover it provides an in-layer Cu–Cl–Cu angle of 180° at ambient conditions (ideal perovskite). Previous specific-heat measurements indicate that $T_N = 13.6$ K [31]. However, the magnetic structure of this compound has not been yet solved, in part due to the difficulties of dealing with the small magnetic moment of Cu^{2+} ($S = 1/2$). Throughout this work we stress the relevance of an adequate characterization on both the crystal and local structure for a proper understanding of magnetic behaviour in layered perovskites.

2. Experimental details

Single crystals of Rb_2CuCl_4 (1–0.1 mm^3) were grown from dried methyl alcohol solutions. A saturated solution of RbCl in methanol was poured into $CuCl_2$ methanol solution, using appropriate stoichiometric amounts of RbCl and $CuCl_2$. After several minutes, red-brownish single crystals precipitate. The orthorhombic *Acam* space group was confirmed by x-ray diffraction (XRD). The room temperature parameters obtained are the same as given elsewhere [46]: $a = 7.187(4)$ Å, $b = 7.197(4)$ Å, and $c = 15.534(6)$ Å. All compounds were handled in a glove box under argon atmosphere in order to avoid hydration. In contact with air, the crystal transforms into the hydrate $Rb_2CuCl_4(H_2O)_2$ phase [47], which is tetragonal ($P4_2/mnm$ space group) with lattice parameters $a = b = 7.596$ Å, and $c = 8.027$ Å. Partial or total hydration can easily be identified by powder XRD and the characteristic yellow-greenish colour.

Neutron diffraction studies at ambient and high pressures were performed at the diffractometer G6.1 of Laboratoire Léon Brillouin at Saclay (France). We used the neutron focusing system described elsewhere [48] and two different high-pressure cells with sapphire anvils [49]. The nuclear and magnetic structures of Rb_2CuCl_4 were determined from the corresponding NPD diagrams, which were analysed using the FULLPROF software package [50].

3. Results and discussion

3.1. Nuclear and magnetic structures of Rb_2CuCl_4

The NPD pattern of Rb_2CuCl_4 obtained at 20 K (figure 2(a)) is associated with nuclear scattering from the paramagnetic phase. It corresponds to the same orthorhombic *Acam* space group determined by XRD at ambient conditions [31]. Below $T_N = 16$ K, the NPD pattern at 1.5 K (figure 2(b)) shows additional weak magnetic contributions. The most relevant corresponds to a new Bragg peak at $2\theta = 17.45°$, which is absent in the paramagnetic phase, and peaks at $2\theta = 35.62°$ and 59.22°. The magnetic Bragg peaks are commensurate with the nuclear unit cell, so they can be related to the primitive orthorhombic cell with a propagation vector $\mathbf{k} = [001]$. The copper ions occupy the 4a site: Cu1 at (0, 0, 0), Cu2 at (1/2, 1/2, 0),

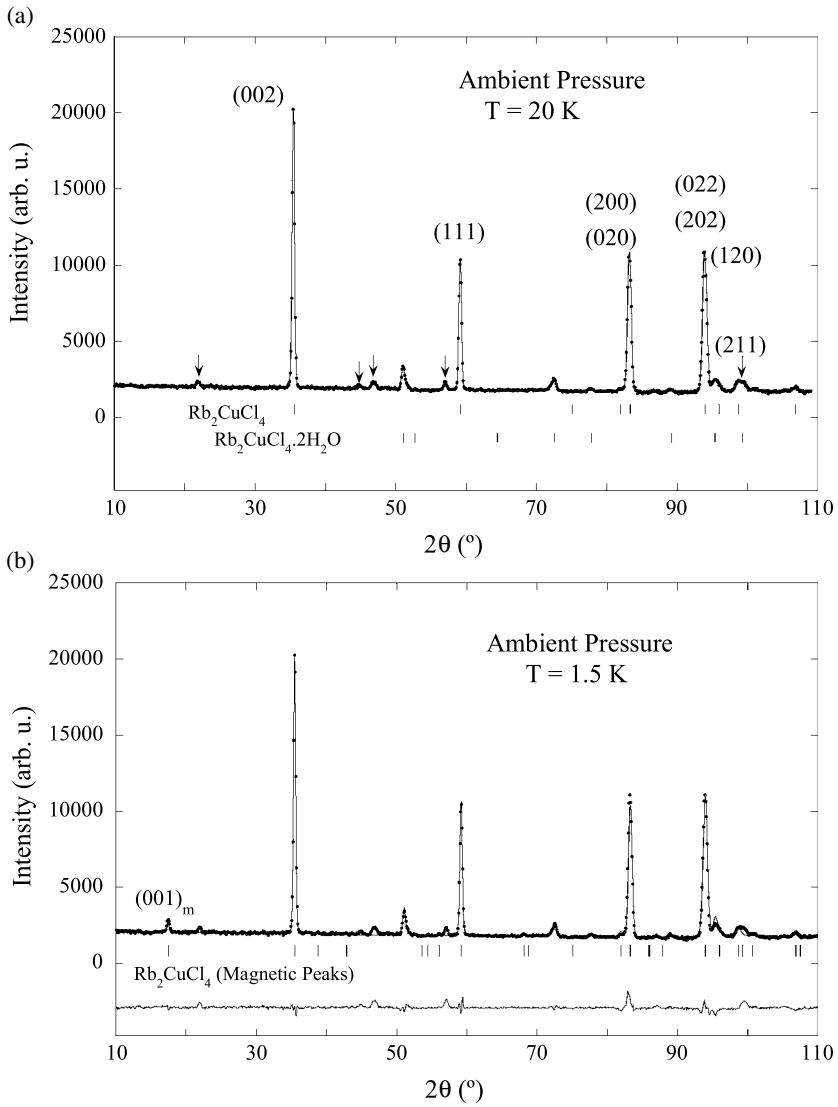

Figure 2. Neutron powder diffraction patterns of Rb_2CuCl_4 obtained at (a) 20 K (paramagnetic phase) and (b) 1.5 K (antiferromagnetic phase). The experimental NPD patterns are compared with the calculated ones obtained by fitting through the FULLPROF software package [50]. Table 3 collects the fitting parameters of the NPD refinement. Neutron wavelength: $\lambda = 4.734$ Å. Arrows indicate Bragg peaks corresponding to small traces of $RbCuCl_3$ and $Rb_3Cu_2Cl_7$.

Cu3 at $(1/2, 0, 1/2)$ and Cu4 at $(0, 1/2, 1/2)$ (figure 1). The refined parameters are listed in table 3.

The magnetic structure (figure 1) consists of two different sublattices associated with adjacent ferromagnetic layers. The crystal symmetry constrains the Cu^{2+} magnetic moment within the (001) plane, which orders antiferromagnetically as is shown in figure 1. The deduced magnetic structure corresponds to *Cx*-type $(+ + - -)$ according to Bertaut's notation [51]. Model refinements converge to a value for the copper magnetic moment along **a** of $\mu_x = 0.83(5)\ \mu_B$, which is slightly reduced with respect to the free-ion moment $\mu = gS = 1.05\ \mu_B$.

Table 3. Structural and magnetic data of Rb_2CuCl_4 at ambient pressure (XRD data) and at 20 and 1.5 K (NPD data). The atom numbering is indicated in figure 1.

Crystal data						
Formula	Rb_2CuCl_4					
Molecular weight	376.3					
Space group	*Acam*, $Z = 4$					
Lattice parameters	$T = 293$ K	20 K	1.5 K			
a (Å)	7.187	7.124	7.122			
b (Å)	7.197	7.127	7.127			
c (Å)	15.534	15.532	15.532			
Volume (Å^3)	803.5	788.6	788.4			
Atomic coordinates[a]	x	y	z			
Cu	0	0	0			
Rb	0	0	0.3584(4)			
Cl1	0.229(1)	0.229(1)	0			
Cl2	0	0	0.1460(6)			
Interatomic distances and angles						
Cu–Cl1	$2x$	2.307(10) Å				
Cu–Cl2	$2x$	2.268(10) Å				
Cu–Cl3	$2x$	2.731(10) Å				
Mean Cu–Cl		2.435(10) Å				
Cu–Cl–Cu		180°				
Magnetic data						
	x	y	z	m_x	m_y	m_z
Cu1	0	0	0	0.835	0.072	0
Cu2	1/2	1/2	0	0.835	−0.072	0
Cu3	0	1/2	1/2	−0.835	−0.072	0
Cu4	1/2	0	1/2	−0.835	0.072	0
Magnetic moment: $\mu = 0.84(5)\ \mu_B$						
Bragg R-factor: $R = 7\%$						

[a] Data at 1.5 K.

We use $S = 1/2$ and an average gyromagnetic factor, $g_{av} = 2.1$, which roughly corresponds to the average value, $g_{av} = (g_\parallel + 2g_\perp)/3$, with $g_\parallel = 2.17$ and $g_\perp = 2.02$ [52]. A refinement test with variable y-component of the magnetic moment results in negligible values along the **b** axis ($\mu_y < 0.07(5)\ \mu_B$, with a large standard deviation).

The results point out the different magnetic behaviour exhibited by Cu^{2+} and Mn^{3+} in layered perovskites. While Rb_2CuCl_4 and the $(C_nH_{2n+1}NH_3)_2CuCl_4$ ($n = 1$–3) series show intralayer ferromagnetism, the series of Mn^{3+} compounds $RbMnF_4$, $NaMnF_4$ and $LiMnF_4$ displays intralayer antiferromagnetism. Tables 1–3 include the magnetic and structural properties of Rb_2CuCl_4 as well as those corresponding to isomorphous series of Cu^{2+} and Mn^{3+} compounds.

3.2. Temperature dependence

The intensity of the $(001)_m$ magnetic Bragg peak, which is associated with the interlayer antiferromagnetic coupling, strongly depends on the thermal fluctuations of the sublattice

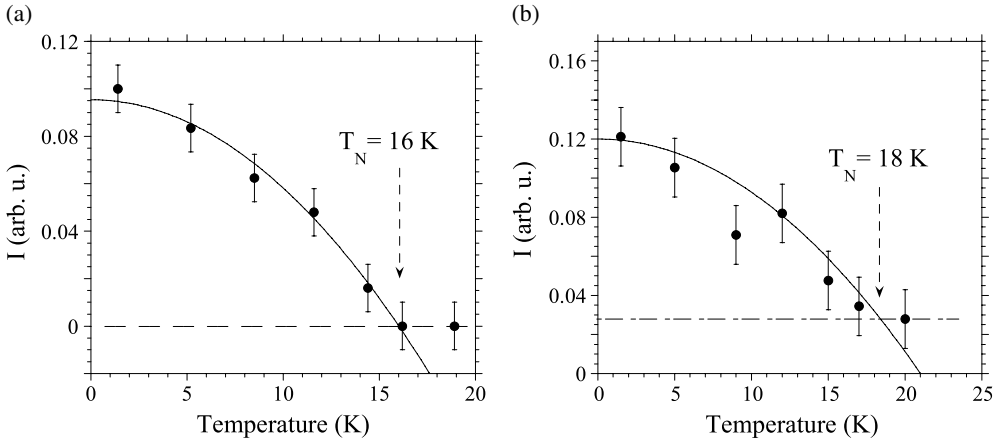

Figure 3. Variation of the integrated intensity of the $(001)_m$ Bragg peak with temperature at (a) ambient pressure and (b) 15 kbar. Full curves correspond to a quadratic fitting of the intensity to the function $I_{(001)}(T) = I(0) - \gamma T^2$. Note that the zero-intensity line in (b) corresponds to the average intensity background obtained from high-temperature diffractograms.

magnetization. The $(001)_m$ intensity is proportional to both the sublattice magnetization and the antiferromagnetic correlation between layers, and therefore its variation with temperature gives directly the Néel temperature (T_N) as is shown in figures 3(a) and (b). The variation of $I(T)$ below $T_N = 16$ K follows a quadratic dependence with temperature which is fairly proportional to the correlation function between nearest-layer sublattice magnetization. The fitting of $I(T)$ to a quadratic function directly provides T_N and confirms the magnetic origin of $(001)_m$ as being due to neutron scattering from Cu^{2+} magnetic moments. A similar procedure was employed by Manaka *et al* [8–10] to determine T_N along the isomorphous $(C_nH_{2n+1}NH_3)_2CuCl_4$ series ($n = 1$–3), and their variation with pressure.

3.3. Neutron diffraction experiments under pressure

Pressure experiments were carried out in a sapphire anvil cell using two different configurations as is indicated in figure 4. Due to preferential orientation in (001) layers, the vertical configuration was unable to provide suitable magnetic Bragg peaks. However, the horizontal configuration enhanced the weak intensity of the $(001)_m$ peak. Nevertheless, the counting time for each NPD pattern, even in that configuration, was 12 h in order to get suitable intensities. This difficulty often occurs in NPD experiments under pressure whenever we deal with weak magnetic moments like Cu^{2+} ($S = 1/2$). At 15 kbar we observe no evidence of other structural or magnetic phases than those observed at ambient pressure. The $(001)_m$ thermal dependence at 15 kbar (figure 3(b)) indicates that T_N increases slightly with pressure. This result is analogous to findings in other Cu^{2+} layer perovskites [8–10]. We measure a variation, $\partial T_N/\partial P = 0.13$ K kbar^{-1}. A comparison of the variation of $T_N(P)$ along layer perovskite series of Cu^{2+} and Mn^{3+} is shown in figure 5.

3.4. Magnetic properties: a structural correlation

Figure 5(a) depicts the variation of critical temperatures, T_C or T_N, for the A_2CuCl_4 series as a function of pressure. The variation of the critical temperature for the $BMnF_4$ series as a function of the Mn–F–Mn tilting angle is given in figure 5(b). The structural and

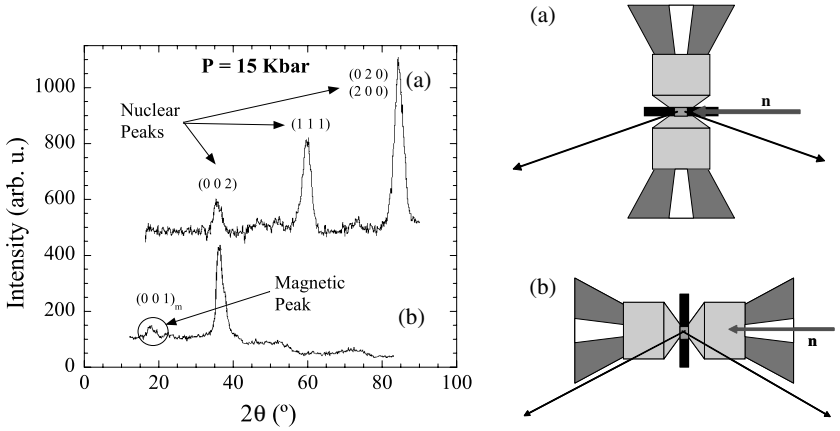

Figure 4. NPD patterns of Rb_2CuCl_4 at 15 kbar corresponding to two geometrical configurations of the sapphire anvil cell (a) and (b). Note the effect of (001) preferential orientation in the NPD patterns. The horizontal configuration (b) was employed for obtaining suitable NPD peaks for magnetic structural analysis as a function of pressure and temperature. Neutron wavelength: $\lambda = 4.734$ Å.

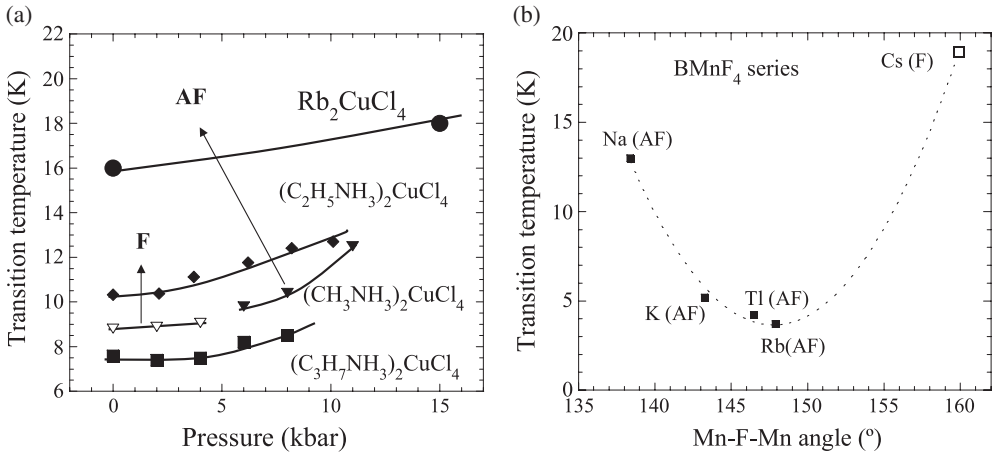

Figure 5. Variation of the Néel (T_N) and Curie (T_C) temperatures along the A_2CuCl_4 series as a function of pressure (a) [8–10], and along the $BMnF_4$ series (b) as a function of the Mn–F–Mn tilting angle [26]. Full and open symbols correspond to antiferromagnetic and ferromagnetic phases, respectively.

magnetic properties of these two series are collected in tables 1 and 2. Note that in all these compounds the critical temperature increases with pressure (or the tilting angle). The $(CH_3NH_3)_2CuCl_4$ ferromagnet becomes antiferromagnetic above 5 kbar [8]. On the other hand, $(C_2H_5NH_3)_2CuCl_4$ and $(C_3H_7NH_3)_2CuCl_4$ compounds are antiferromagnetic. Nevertheless, $(C_3H_7NH_3)_2CuCl_4$ exhibits a weak intralayer spin-canting ferromagnetism along **b**, which is suppressed by applying pressure above 8.1 kbar [10]. In $(C_2H_5NH_3)_2CuCl_4$, however, pressure induces a weak ferromagnetism along **c** above 6 kbar at low temperature that remains up to 25 kbar [9]. The occurrence of pressure-induced weak ferromagnetism was associated with spin-canting due to asymmetric exchange interactions [53, 54]. An important

conclusion is that the asymmetric exchange yielding ferromagnetism is likely related to tilts of the $CuCl_6$ octahedra.

The $BMnF_4$ series, together with the pure antiferromagnetic behaviour exhibited by the ideal layer perovskite Rb_2CuCl_4, support this idea. The absence of tilts in Rb_2CuCl_4 enhances the intralayer ferromagnetic coupling but favours an interlayer antiferromagnetic interaction. This behaviour is, however, opposite to that shown by the $BMnF_4$ series (table 2). The magnetism of the Mn^{3+}-compound series is mainly governed by the intralayer Mn–Mn exchange interaction. Actually, the sign and magnitude of intralayer superexchange constant J rely on the Mn–F–Mn tilting angle, α, in such a way that either ferromagnetism or antiferromagnetism occurs depending on whether α is higher or lower than the critical value, $\alpha_c = 147°$ [17] (figure 5(b) and table 2). Within this model, the decrease of T_C with pressure in $CsMnF_4$ and the switch from ferromagnetism to antiferromagnetism is explained by pressure-induced tilts. We can conclude that the reduction of crystal volume either along the $BMnF_4$ series (B: Cs $\rightarrow$ Rb $\rightarrow$ Tl $\rightarrow$ Na $\rightarrow$ Li) or induced by hydrostatic pressure [17, 26], favours antiferromagnetic exchange interaction.

An analogous structural correlation could be extrapolated to the A_2CuCl_4 (A: $C_nH_{2n+1}NH_3$, Rb) series provided that the tilting Cu–Cl–Cu angles were similar. The intralayer Cu–Cu ferromagnetic exchange is dominant since A_2CuCl_4 compounds are nearly ideal perovskites: $\alpha > 165°$ (table 1). Consequently, we expect that the 3D magnetic ordering is mainly governed by the interlayer exchange. Following our previous analysis, the structural requirements for a compound to be ferromagnetic or antiferromagnetic are not yet fully understood. Although the 3D ferromagnetism of $(CH_3NH_3)_2CuCl_4$ suggests that it is related to shorter interlayer distances, the NPD experiments on Rb_2CuCl_4 reported in this work rule out this possibility. In trying to establish magneto-structural correlations in A_2CuCl_4, we realize that the variations of both the interlayer and intralayer exchange interactions as a function of pressure are crucial to account for the ample variety of magnetic behaviour.

We have searched for correlations between the exchange interactions and structural parameters involving Cu–Cu distances and Cu–Cl–Cu tilting angles simultaneously. The correlations are quantitative for $|J'/J|$ along the A_2CuCl_4 series. Interestingly, the logarithm of this ratio scales fairly well with the parameter $f = [1 - p\cos^2(\alpha)]/(d_2/d_1)^n$, as shown in figure 6(a). The best linear fit was obtained for $p = 0.83$ and $n = 4.5$. This result stresses the relevance of both the Cu–Cl–Cu tilting and intra- and interlayer Cu–Cu distances to explain the magnetic properties of the series. In particular, this correlation reconciles the different magnetic behaviour of Rb_2CuCl_4 and $(CH_3NH_3)_2CuCl_4$. The reason for the tilting favouring interlayer ferromagnetic coupling is probably due to structural changes towards ideal Cu–Cl $\cdots$ Cl–Cu arrangements yielding ferromagnetism. However, it must be noted that although tilts probably decrease the intralayer Cu–Cl–Cu ferromagnetic exchange, they are not effective enough to destroy it.

Figure 6(b) shows the relation between the critical temperature (T_C or T_N) and the structural parameter β, defined as $\beta = \sin(\alpha)/(d_2/d_1)$, for the A_2CuCl_4 and $BMnF_4$ series, and K_2CuF_4. Interestingly, β increases with the tilting angle and reducing the interlayer Cu–Cu distance, analogously to the f parameter (see above). Note that the number of compounds included in these two correlations is limited by the structural and magnetic data available in the literature.

β allows us to draw a common phase diagram for the layered JT compounds (figure 6(b)). Depending on β, we find three different magnetic regions associated with a distinct magnetic behaviour. For $\beta < 0.11$ (interlayer AF), the compounds are 3D antiferromagnetic but ferromagnetic within the layers. Ferromagnetism occurs for $0.11 < \beta < 0.35$, while the region $\beta > 0.35$ (intralayer AF) is associated with compounds exhibiting the highest tilting

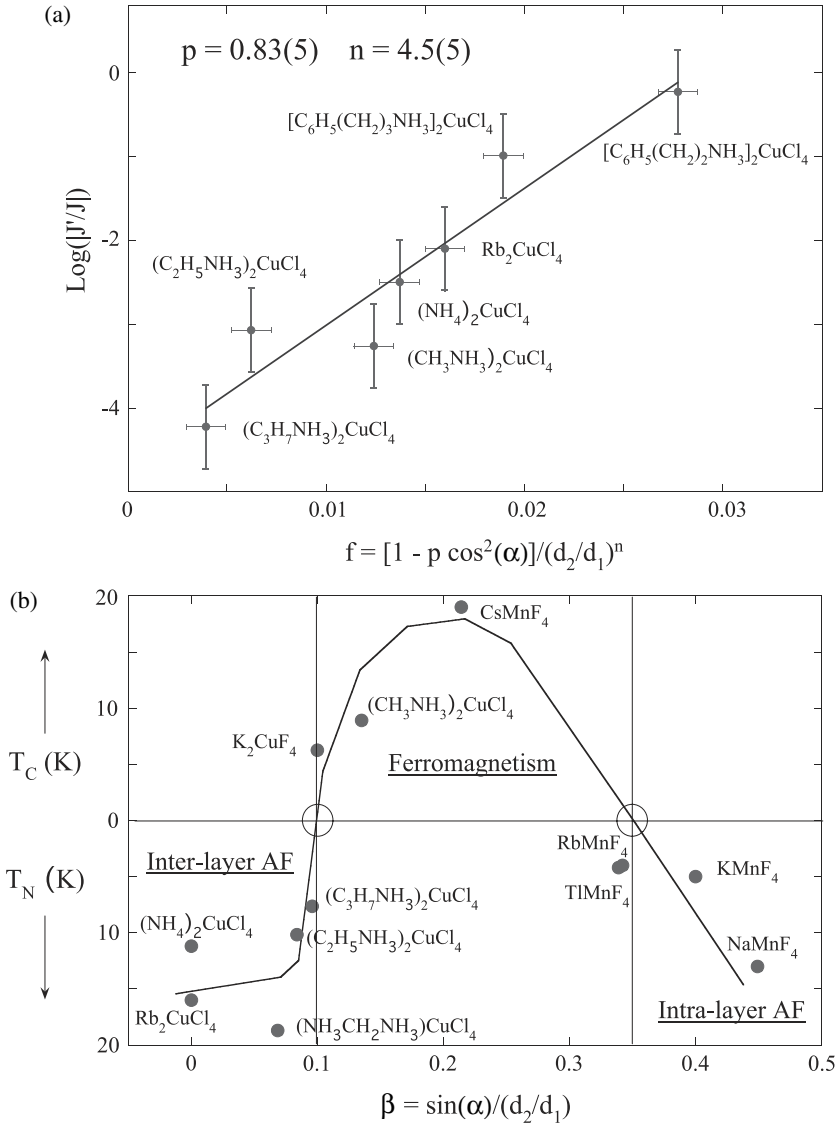

Figure 6. Magneto-structural correlations: (a) semilog plot of the interlayer-to-intralayer J'/J exchange coupling in A_2CuCl_4, and (b) critical temperatures (T_N or T_C) along the A_2CuCl_4 and $BMnF_4$ series, and K_2CuF_4 as a function of structural parameters involving the tilting angle and the Cu–Cu distances (see section 3.4 and tables 1 and 2).

angles ($\alpha < 147°$). In this region, the magnetic properties are governed by the intralayer exchange interactions. With the exception of $CsMnF_4$, the $BMnF_4$ series belongs to this region.

Figure 6(b) suggests that the pressure-induced antiferromagnetism is related not only to a decrease of intra- and interlayer Cu–Cu distances, but also to tilts of the JT-distorted octahedra both leading to intralayer antiferromagnetism. However, a confirmation of this behaviour deserves additional structural studies under pressure.

4. Conclusions

We have shown that Rb_2CuCl_4 is an intralayer ferromagnet but exhibits 3D antiferromagnetism, $T_N = 16$ K, associated with interlayer antiferromagnetic exchange interaction, J'. Pressure increases T_N to 18 K on passing from ambient pressure to 15 kbar. A comparison of the magnetic properties of this compound and the A_2CuCl_4 series reveals that the tilting angle of the JT-distorted octahedra plays a key role in the occurrence of either 3D antiferromagnetic or ferromagnetic order. In particular, the antiferromagnetism of Rb_2CuCl_4 is related to the ideal layer perovskite structure ($\alpha = 180°$) in spite of the short interlayer distance. We have established a quantitative correlation between the exchange interactions and structural parameters involving both the tilting angle and the Cu–Cu distances. From this correlation, we stress the relevance of octahedron tilts on the magnetic behaviour of layered perovskites. We have shown that the critical temperatures (T_N or T_C) can be represented in a phase diagram for the whole series using the structural parameter β. The variation of the magnetic properties with pressure can eventually be explained on the basis of the proposed model. However, an adequate structural characterization at both short- and long-range levels is necessary in order to establish precise structural correlations.

Acknowledgments

Financial support from the Spanish MCyT (Project No BFM2001-0695) is acknowledged. The neutron diffraction experiments under pressure were done under experimental proposal at the Laboratoire Léon Brillouin [Experiment Project No 6419]. One of the authors (FA) thanks the Ministerio de Ciencia y Tecnología (MCyT) for a FPI Research Grant (No FP99, Project No PB98-0190).

References

[1] de Jongh L J and Miedema A R 1974 *Adv. Phys.* **23** 1
[2] Rüdorff W, Lincke G and Babel D 1963 *Z. Anorg. Allg. Chem.* **320** 150
[3] Sasaki S, Narita N and Yamada I 1995 *J. Phys. Soc. Japan* **64** 2701
[4] Willett R D, Jardine F H, Rouse I, Wong R J, Landee C P and Numata M 1981 *Phys. Rev.* B **24** 5372
[5] Hitchman M A 1994 *Comment. Inorg. Chem.* **15** 197
[6] Valiente R and Rodriguez F 1999 *Phys. Rev.* B **60** 9423
[7] de Jongh L J 1976 *Physica* B **82** 247
[8] Manaka H, Yamada I, Nishi M and Goto T 2001 *J. Phys. Soc. Japan* **70** 1390
[9] Manaka H, Yamada I, Nishi M and Goto T 2001 *J. Phys. Soc. Japan* **70** 241
[10] Manaka H, Yamada I and Goto T 2002 *J. Phys. Soc. Japan* **71** 2822
[11] Narita N and Yamada I 1996 *J. Phys. Soc. Japan* **65** 4054
[12] Sekine T, Okuno T and Awaga K 1996 *Chem. Phys. Lett.* **249** 201
[13] Drumheller J E, Dickey D H, Reklis R P and Zaspel C E 1972 *Phys. Rev.* B **5** 4631
[14] Moritomo Y and Tokura Y 1994 *J. Chem. Phys.* **101** 1763
[15] Losee D B and Hatfield W E 1974 *Phys. Rev.* B **10** 1122
[16] Estes W E, Losee D B and Hatfield W E 1980 *J. Chem. Phys.* **72** 630
[17] Palacio F and Moron M C 1993 *Research Frontiers in Magnetochemistry* ed C J O'Connor (Singapore: World Scientific)
[18] Nuñez P, Tressaud A, Grannec J, Hagenmuller P, Massa W, Babel D, Boireau A and Soubeyroux J L 1992 *Z. Anorg. Allg. Chem.* **609** 71
[19] Molinier M, Massa W, Khairoun S, Tressaud A and Soubeyroux J L 1991 *Z. Naturf.* b **46** 1669
[20] Köhler P, Massa W, Reinen D, Hoffman B and Hoppe R 1978 *Z. Anorg. Allg. Chem.* **446** 131
[21] Aguado F, Rodriguez F and Nuñez P 2003 *Phys. Rev.* B **67** 205101
[22] Rodriguez F and Aguado F 2003 *J. Chem. Phys.* **118** 10867 and references therein
[23] Massa W and Steiner J 1980 *J. Solid State Chem.* **32** 137

[24] Khomskii D I and Kugel K I 1973 *Solid State Commun.* **13** 763
[25] Ishizuka M, Henmi S, Endo S, Moron M C and Palacio F 1999 *J. Magn. Magn. Mater.* **196/197** 440
[26] Moron M C, Palacio F, Clark S M and Paduan-Filho A 1995 *Phys. Rev.* B **51** 8660
[27] Hidaka M, Inoue K, Yamada I and Walker P J 1983 *Physica* B **121** 343
[28] Yamada I 1972 *J. Phys. Soc. Japan* **33** 979
[29] Li W H, Pery C H, Sokoloff J B, Wagner V, Chen M E and Shirane G 1987 *Phys. Rev.* B **35** 1891
[30] Dance J M, Grannec J and Tressaud A 1976 *C. R. Acad. Sci.* C **283** 115
[31] Witteveen H T 1974 *Physica* **71** 204 and references therein
[32] Willett R D 1964 *J. Chem. Phys.* **41** 2243
[33] Steadman J P and Willett R D 1970 *Inorg. Chim. Acta* **40** 367
[34] Steijger J J M, Frikkee E, de Jongh L J and Huiskamp W J 1984 *Physica* B **123** 284
[35] Barendregt F and Schenk H 1970 *Physica* **49** 465
[36] Dupas A, Le Dang L, Renard J P, Veillet P, Daoud A and Perret R 1976 *J. Chem. Phys.* **65** 4099
[37] Snively L O, Seifert P L, Emerson K and Drumheller J E 1979 *Phys. Rev.* B **20** 2101
[38] Snively L O, Tuthill G F and Drumheller J E 1981 *Phys. Rev.* B **24** 5349
[39] Soos C G, McGregor K T, Cheung T T P and Silverstein A J 1977 *Phys. Rev.* B **16** 3036
[40] Moron M C, Palacio F and Rodriguez-Carvajal J 1993 *J. Phys.: Condens. Matter* **5** 4509
[41] Wandner K H and Hope R 1987 *Z. Anorg. Allg. Chem.* **546** 113
[42] Ishizuka M, Yamada I, Amaya K and Endo S 1996 *J. Phys. Soc. Japan* **65** 1927
[43] Mitrofanov V Ya, Mikiforov A and Shashkin S Yu 1997 *Solid State Commun.* **104** 499
[44] Manaka H, Yamada I, Kitazawa T, Kobayashi M, Ishizuka M and Endo S 1997 *J. Phys. Soc. Japan* **66** 2989
[45] Ishizuka M, Terai M, Hidaka M, Endo S, Yamada I and Shimomura O 1998 *Phys. Rev.* B **57** 64
[46] Witteveen H T, Jongejan D L and Brandwijk V 1974 *Mater. Res. Bull.* **9** 345
[47] Waizumi K, Masuda H, Ohtaki H, Burkov K A and Chernykh L 1992 *Acta Crystallogr.* C **48** 1374
[48] Goncharenko I N, Mirebeau I, Molina P and Böni P 1998 *Physica* B **234** 1047
[49] Goncharenko I N, Glazkov V P, Irodova A V, Lavrova O A and Somenkov V A 1992 *J. Alloys Compounds* **179** 253
[50] Rodriguez-Carvajal J 1993 *Physica* B **192** 55
[51] Bertaut E F 1968 *Acta Crystallogr.* A **24** 217
[52] Wong R J H, Willett R D and Drumheller J E 1981 *J. Chem. Phys.* **74** 6018
[53] Goodenough J B 1963 *Magnetism and the Chemical Bond* (New York: Wiley–Interscience)
[54] Kanamori J 1959 *J. Phys. Chem. Solids* **10** 87